Optical coherence tomography (OCT) to image active and inactive retinoblastomas as well as retinomas

Oleg Nadiarnykh,[1] Nuray A. McNeill-Badalova,[2] (iD) Marie-Claire Gaillard,[3] (iD) Machteld I. Bosscha,[2] Armida W.M. Fabius,[2] Frank D. Verbraak,[2] Francis L. Munier,[3] Johannes F. de Boer[1,2] and Annette C. Moll[2]

[1]Department of Physics and Astronomy, VU University, HV Amsterdam, The Netherlands
[2]Department of Ophthalmology, Amsterdam UMC, location VUMC, HV Amsterdam, The Netherlands
[3]Department of Ophthalmology, Jules-Gonin Eye Hospital, Lausanne, Switzerland

ABSTRACT.

Purpose: To illustrate Optical Coherence Tomography (OCT) images of active and inactive retinoblastoma (Rb) tumours.

Methods: Current observational study included patients diagnosed with retinoblastoma and retinoma who were presented at Amsterdam UMC and Jules-Gonin Eye Hospital, between November 2010 and October 2017. Patients aged between 0 and 4 years were imaged under general anaesthesia with handheld OCT in supine position. Patients older than 4 years were imaged with the conventional OCT (Heidelberg Engineering, Heidelberg Spectralis, Germany). All patients included were divided into two groups: active and inactive tumours (retinoma and regression patterns). Patients' medical records and OCT images were analysed during meetings via discussions by ophthalmologists and physicists.

Results: Twelve Dutch and 8 Swiss patients were divided into two groups: 2 patients with active tumour versus 18 patients with inactive tumour. Subsequently, inactive group could be divided in two groups, which consisted of 10 patients with retinoma and 8 patients with different regression pattern types. Of all included patients, 15 were male (75%). Median age at diagnosis was 18.0 months (range 0.19–715.2 months). A total of 12 retinoblastoma (active and inactive) and 8 retinoma foci were investigated by OCT. No distinction could be made between active and inactive tumours using only OCT.

Conclusion: Optical coherence tomography alone cannot distinguish between active and inactive Rbs. However, handheld OCT adds useful information to the established imaging techniques in the monitoring and follow-up of retinoblastoma patients. With this study, we provide an overview of OCT images of active and inactive Rbs.

Key words: optical coherence tomography – paediatric oncology – regression patterns – retina – retinoblastoma – retinoma

Introduction

Retinoblastoma (Rb) is the most common malignant paediatric ocular tumour with an incidence of 1:17 000 (Moll 1996; Moll et al. 1997; Shields et al. 2015). With the current standard of care the survival rate of retinoblastoma cases is around 90–99% in developed countries (Jenkinson 2015). Patients with retinoblastoma must be frequently monitored under anaesthesia before the age of five for early detection of new or relapsed tumours, as well as for the treatment and detection of side effects, in order to reach these survival rates (Yun et al. 2011). Retinoblastoma can exhibit different regression patterns after treatment. Tumour regression patterns were originally defined as a remnant lesion visible after external beam radiotherapy (EBRT) (Dunphy 1964; Abramson et al. 1991; Singh et al. 1993), but was later also applied for tumour remnants after chemoreduction (Shields et al. 2009).

While retinoblastoma is a rapidly growing malignancy, retinoma is a benign retinal tumour characterized by the absence of growth or shrinkage over time (Dimaras et al. 2008; Shah et al. 2011). The term 'retinoma' was first introduced in the literature by Gallie and colleagues (Gallie et al. 1982) based on the observations of 30 patients. It appears identical to regressed tumours post-EBRT or chemoreduction except that no

treatment needs to be applied (Abouzeid et al. 2012).

Ocular oncologists use wide-angle retinal photography and indirect ophthalmoscopy for retinoblastoma management (Haye et al. 1989). With these tools it can be challenging to detect the presence of active tumour tissue in need of additional treatment. Due to the limited real-time diagnostic options ophthalmologists currently often rely on monthly monitoring the patients at risk under general anaesthesia. Consequently, critical time might be lost in case of tumour (re)growth. Early detection and characterization could avoid (unnecessary) harmful treatments and increase effectiveness of focal treatment options that preserve better eye functionality.

Optical coherence tomography (OCT) is an established three-dimensional imaging technique in ophthalmologic clinical practice with demonstrated ability to improve diagnostic assessment and treatment decisions in real time. Recently, it has been expanded to a handheld ophthalmic OCT configuration required for paediatric retinoblastoma patients under anaesthesia (Rootman et al. 2013; Lee et al. 2016). A number of authors suggested that adding OCT imaging into the management decisions of retinoblastoma could be essential (Shields et al. 2005; Yousef et al. 2012; Rootman et al. 2013; Cao et al. 2014; Mallipatna et al. 2015; Saktanasate et al. 2015; Berry et al. 2016; Park et al. 2017; Shields & Shields 2017; Soliman et al. 2017; Gaillard et al. 2018; Malik et al. 2018; Stathopoulos et al. 2018). Handheld OCT has been successfully utilized in diagnosis (Rootman et al. 2013), detection of clinically invisible smaller tumours (Rootman et al. 2013; Saktanasate et al. 2015; Berry et al. 2016), follow-up of treatment results (Park et al.2017; Gaillard et al. 2018), assessment of optic nerve invasion (Yousef et al. 2012; Mallipatna et al. 2015; Fabian et al. 2017) and disease management decisions (Soliman et al. 2017) for paediatric retinoblastoma patients (under the age of four).

Currently, conventional OCT (Heidelberg Engineering, Heidelberg Spectralis, Germany) is a widely used imaging tool, especially in vitreoretinal field. Only one commercial system with handheld spectral domain OCT (HHSD-OCT), (two generations of Bioptigen Envusu C2200/Envisu C2300, Leica Microsystems Morrisville, NS) operating at the central wavelength of 860 nm, is available at only a few specialized centres worldwide. Therefore, the number of handheld OCT studies in young retinoblastoma patients is limited and more studies are needed. For this clinical study, we developed a novel handheld Swept Source OCT system with 1050-nm central wavelength for a deeper penetration into the tumour.

We aimed to demonstrate an overview of OCT images of active and inactive retinoblastoma tumours, different regression patterns and retinoma. The OCT images made with the newly developed handheld imaging system for retinoblastoma patients (aged between 0 and 4 years, under general anaesthesia), are shown together with the conventional OCT system (older patients, > 4 years, not requiring anaesthesia).

Materials and Methods

Participants

The present study is an observational study including retinoblastoma and retinoma patients from two centres (Amsterdam UMC and the Jules-Gonin Eye Hospital). All patients aged between 0 and 4 years old were imaged under anaesthesia with the novel handheld OCT. Patients older than or equal to 4 years were imaged while seated with the conventional OCT (Heidelberg Spectralis).

Inclusion and exclusion criteria

Dutch patients
Patients ($n = 12$) diagnosed with retinoblastoma or retinoma and seen between November 2014 and October 2017 during general anaesthesia sessions were included. Exclusion criteria were peripheral tumours, big tumours (exceeding the focusing range and axial field of view of the system due to their extension towards the cornea), total retinal detachment at the first clinical presentation or due to lack of informed consent from the guardians.

Swiss patients
All cases of retinoma ($n = 8$) presenting from November 2010 to December 2015 at the Jules-Gonin Eye Hospital were retrospectively reviewed with respect to fundus and OCT (Heidelberg Spectralis) imaging. Exclusion criteria were: prior probatory treatment; chemotherapy for retinoblastoma; OCT scans imaging of low quality or failed to achieve due to tumour size, retinal detachment or anterior segment lesions.

Data collection and processing

The following clinical data were collected via patient medical charts for all the included patients: gender, age at diagnosis, laterality at diagnosis (uni-, bi- or trilateral), heredity, information regarding the scanned eyes and scanned tumours, number of tumours at diagnosis, tumour growth pattern, tumour type (active tumour, slow growing tumour, retinoma or regression types), tumour location, staging of the tumour (according to International Intraocular Retinoblastoma Classification (IIRC) and the American Joint Committee on Cancer's (AJCC) TNM-classification system) (Linn Murphree 2005; Sobin et al. 2010), therapy information and follow-up data. All included tumours were divided into active and inactive lesions, with active ones subdivided into tumours at diagnosis and active tumours during therapy. Inactive tumours were divided into: regression pattern types and retinomas. Regression pattern types are defined according to Wills Eye Institute classification: type 0 – no tumor remnant/no retinal scar visible, type I – completely calcified tumour remnant (cottage cheese scar), type II – fish flesh tumour remnant (completely non-calcified tumour remnant), type III – combination of calcified and fish flesh tumour remnant and type IV – flat chorioretinal scar (Shields et al. 2009). Retinomas were subdivided using the same classification.

The OCT scans with the handheld imaging system were analysed at meetings and discussed by ophthalmologists and physicists using the inclusion and exclusion criteria. We additionally reviewed all the combined clinical and imaging data: the eligible OCT scans and retina images (Retcam; Optos). Data and images are presented in a descriptive form. No statistics were performed in the current study.

Fig. 1. Picture of the novel handheld OCT device during anaesthetic hours of Rb patients.

Handheld OCT imaging procedure

Handheld OCT imaging (Fig. 1) was performed during the routine clinical sessions for Rb patients (under the age of 4 years) in supine position under inhalation anaesthesia. Working distance of the ophthalmic lens is 1 cm allowing for working with no contact with patient's cornea during imaging. Artificial tears eye gel was applied during imaging according to a standard clinical practice. The laser beam entered the eye through the pupillary centre and the optimal focusing was determined based on a continuously acquired B-scan. To achieve the best quality, the reference arm was adjusted and the focusing lens, followed by the polarization compensator to offset the depolarizing effect inside the patient's eye. A coarse en-face preview guided the physician to the desired region of interest and indicated if rescanning was needed to improve the quality of the images. The complete technical description of our HHSD-OCT is given in the angiography study (Nadiarnykh et al. 2019). The non-contact imaging system provided lateral resolution of $10–18 \mu m$ dependent on focusing with the lateral field of view up to ± 14 degrees, while axial resolution was below $8 \mu m$. For the current study, we used only intensity-based structural OCT imaging.

Results

Overall, 20 eyes from 12 Dutch and 8 Swiss patients were included in this study. Baseline characteristics of the study population are summarized in Table 1. Of those, 15 patients were

male (75%). Median age at diagnosis for the whole study population was 18.0 months (range 0.19–715.2 months). Only 4 patients (20%) had non-hereditary retinoblastoma (unilateral cases without germline mutation), while 10 patients (50%) were affected with sporadic hereditary Rb and 6 (30%) with a familial hereditary Rb. At imaging, locations of the tumours were macula ($n = 8$, 40%), macula–equator ($n = 5$; 25%), equator ($n = 3$; 15%), ora serrata ($n = 1$; 5%), and equator–ora ($n = 3$; 15%). Most of the eyes were group B eyes ($n = 16$; 80%). Only two tumours were staged as a group A (Linn Murphree 2005) lesion. Both of them showed a flat lesion on OCT imaging. Characteristics of patients are listed in Table 2. Additional overview with a full description per patient is provided in an online supplementary material in Appendix S1. OCT and funduscopy images are demonstrated in figures (Figs 2–4). Additional results regarding fundus and OCT images are presented in an supporting information (Appendix S2).

Active tumours

Two patients, one male and one female, had an active tumour during the scanning (Fig. 2 and Appendix S1: patients HH1 and HH2). Both of them were affected with hereditary bilateral retinoblastoma and were scanned with the novel handheld OCT at a young age (2 and 3 months). These tumours were located in the macula. One of them is scanned at presentation (patient HH1), while the other was active during the follow-up after therapy (patient HH2).

Inactive tumours – regression patterns

Eighteen patients were included for the inactive tumour group. We scanned eight patients with regression patterns as a remnant after therapy (Fig. 3 and Appendix S1). Figure 3B and F both show irregular surface with calcifications in the centre, characterized by light scattering (observed as white shadow under black lesions). Figure 3D shows a homogenous lesion underneath a smooth surface, showing a regression pattern type 3 in left eye of a 1.5-year-old boy whose left eye was treated with one cycle of intra-arterial chemotherapy and laser therapy.

Inactive tumours – retinomas

Ten patients were scanned with retinoma, which showed no growth over time (Fig. 4 and Appendix S2). The majority of these (9 out of 10, 90%) were scanned with Heidelberg OCT. Eight patients (80%) with retinoma had no prior treatments. Two remaining patients (20%) were initially considered having retinoblastoma and were subsequently diagnosed with retinoma when the lesion did not respond to the therapy and showed no growth over time (patients HH4 and SH1).

Table 1. Descriptive table of the whole study population

Characteristic	Total, $n = 20$
Age at diagnosis	*Months*
Mean	105.5
Median	18
Range	0.3–715.2
Gender	*No (%)*
Male	15 (75)
Female	5 (25)
Laterality	*No (%)*
Unilateral	8 (40)
Bilateral	12 (60)
Scanned eye	*No (%)*
Right eye	11 (55)
Left eye	9 (45)
Heredity	*No (%)*
Non-hereditary, sporadic	4 (20)
Hereditary, sporadic	10 (50)
Hereditary, familial	6 (30)
Age at OCT	*Months*
Mean	154.4
Median	59
Range	3–715.2
Type tumour scanned	*No (%)*
Active	2 (10)
Retinoma	10 (50)
Regression pattern types	8 (40)

Table 2. Characteristics of participants (per tumour type)

Type tumour	n	Gender	Heredity	Imaging	Location	Staging†
Active	2	M:1, F:1	Sporadic: 1, Familial: 1	HHSD:2	Macula:2	pT1b pN0 cM0:2
Regression type 1*	1	M:1	Sporadic:1	HHSD:1	Macula:1	pT1c pN0 cM0:1
Regression type 2*	3	F:1, M:2	Sporadic:1, Familial: 2	HHSD: 3	Macula: 3	pT1b pN0 cM0:2, pT1c pN0 cM0:1
Regression type 3*	3	F:1, M:2	Sporadic:2, Familial: 1	HHSD:3	Macula-equator:3	pT1b pN0c M0:2, pT1c pN0 cM0:1
Regression type 4*	1	M:1	Sporadic:1	HHSD:1	Macula-equator:1	pT1a pN0 cM0:1
Retinoma type fish flesh	3	M:3	Sporadic: 2, Non-hereditary:1	HHSD:1, SH: 2	Macula:2, Equator:1	pT1b pN0 cM0:3
Retinoma type flat	2	F:1, M:1	Familial: 2	SH: 2	Equator:1, Equator-ora:1	pT1a pN0 cM0:1, pT1b pN0 cM0:1
Retinoma type mixed	4	F:1, M:3	Sporadic: 2, Non-hereditary: 2	SH:4	Ora:1, equator:1, Macula-equator:1, Equator-ora: 1	pT1b pN0 cM0:4
Retinoma type calcified	1	M:1	Non-hereditary: 1	SH:1	Equator-ora:1	pT1b pN0 cM0:1

F = female, HHSD = Handheld Spectral Domain OCT, M = male, SH = Spectralis Heidelberg OCT.
Type tumour: Regression pattern types.
*Regression pattern types [Shields et al. 2009]: Type 0 = No tumour remnant; Type 1 = Calcified tumour remnant; Type 2 = Fish flesh; Type 3 = Mix; Type 4 = Flat.
†Staging was according to the Union for International Cancer Control/American Joint Committee on Cancer (UICC / AJCC) Tumour, Node, Metastasis (TNM) categories and stages (7th Edition).

Figure 4B shows an OCT image of the left eye of a 27-year-old male. Heidelberg OCT shows clear characteristics of a flat type retinoma. Besides a slightly irregular surface with a flat centre, atrophy of the retina layers up until retinal pigment epithelium are observed. Figure 4D demonstrates an OCT image of fish flesh retinoma, a homogenous tumour mass, not responding to any therapy. Three blood vessels are observed on the upper surface of the mass, characterized by the shadowing underneath the vessels. It must be noted that no signs of calcification are seen in the OCT image of this tumour remnant. After a longer follow-up time, the lesion got smaller in size, showing similar characteristics as observations in regression type 2 (fish flesh remnant).
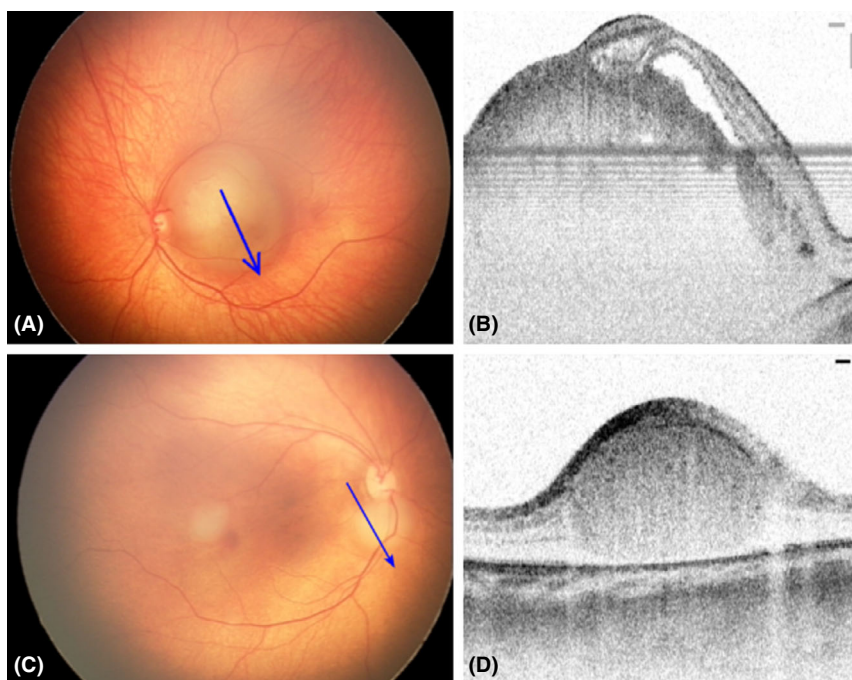
Additional findings

OCT characteristics were further analysed in an attempt to distinguish active and inactive tumours, but no distinct features could be identified to differentiate them (data not shown).
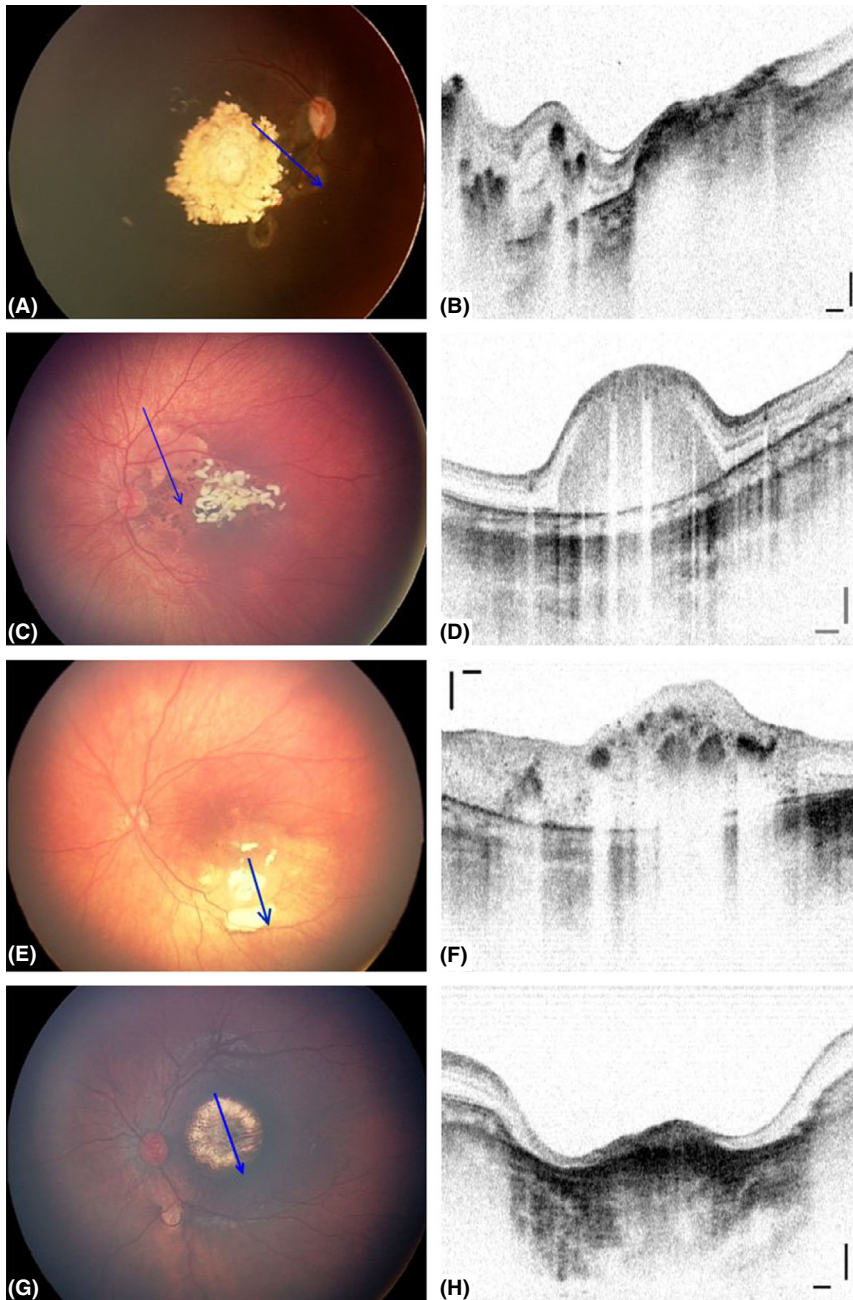
Most of the handheld OCT images were easy to interpret and confirmed generally the clinical signs seen in fundus photography. A couple of OCT images were ambiguous, mostly due to a bigger tumour as observed in Fig. 4F and H or because of the location of the tumour.

Fig. 2. Fundus picture and OCT scan of patients with active tumour. *Active at diagnosis – Patient HH1:* (A) Fundus picture of the left eye at the diagnosis located in the centre of the macula. (B) HHSD-OCT scans of the tumour in the left eye at the diagnosis showing an (endophytic and) exophytic tumour with calcifications and a small retinal detachment. *Active during therapy – Patient HH2:* (C) Fundus picture of the right eye 4 weeks after the diagnosis and one cycle of systemic Carboplatin. (D) HHSD-OCT image of the right eye demonstrating a vital tumour 2 months after diagnosis (and two cycles of systemic Carboplatin).

Discussion

Optical coherence tomography is a non-invasive imaging technique based on interference of reflected laser light, which is used to obtain cross-sectional images of the posterior retina. The conventional OCT (with a chinrest

Fig. 3. Fundus picture and OCT scan of patients with inactive tumours (regression patterns). *Regression pattern type I – Patient HH11:* (A) Fundus picture and (B) HHSD-OCT scans of the right eye. After therapy, a fully calcified remnant was observed. *Regression pattern type II –* Fundus picture and HHSD-OCT scan. (C,D) Left eye in *patient HH5;* Ten months after the detection and therapy. Blue arrow pointing to the lesion in the left eye in *patient HH5* occurring after one cycle of intra-arterial chemotherapy and not reacting to laser therapy. *Regression pattern type III –* (E,F) Fundus picture and HHSD-OCT of *Patient HH8* Mass in the left eye. Regression of the lesion in reaction to Ruthenium plaque, after systemic chemotherapy and laser. Combination of calcified and fish flesh remnant is seen. *Regression pattern IV –* (G,H) Fundus picture and HHSD-OCT of left eye in *patient HH10;* flat lesion (atrophic) after treatment with chemotherapy. Blue arrow pointing to the lesion in fundus picture, lesion stays stable over time.

and no general anaesthesia) in retinoblastoma patients was first described in literature by Shields and associates in 2004 (Shields et al. 2004). They investigated the role of conventional OCT in fundus tumours in a retrospective single-centre case series of 44 retinoblastoma patients younger than 18 years. Authors compared their findings with OCT to those of clinical examination and ultrasonography. They showed that in comparison with clinical examination, OCT is more sensitive in the detection of macular pathology, surface wrinkling maculopathy, macular oedema, subfoveal fluid and retinal thinning. Furthermore, in comparison with ultrasonography, OCT tends to be more sensitive in detection of surface wrinkling maculopathy, non-cystoid macular oedema and subfoveal fluid.

At present, OCT is a widely used imaging modality in ophthalmology, but its use cannot be implemented easily for young infants examined in supine position under anaesthesia, without the adapted handheld technique, first introduced by Scott et al. (2009).

In the present study, we implemented a new handheld OCT imaging system together with the conventional OCT imaging for retinoblastoma and retinoma patients. We aimed to document OCT imaging findings in active and inactive retinoblastoma as well as in retinoma. To the best of our knowledge, this is the first comprehensive study in literature giving an overview for retinoblastoma patients systematically demonstrating different regression patterns as well as retinomas based on images made with handheld and conventional OCT.

Recently, Malik and associates described the importance of handheld OCT in an observational case report (Malik et al. 2018). A 15-month-old girl was diagnosed with bilateral retinoblastoma after presenting with leukocoria in the left eye. Macular tumour in the left eye was unresponsive to chemotherapy, but reacted well to plaque radiotherapy, which could be confirmed by imaging with the handheld OCT. The authors underline the critical role of handheld OCT in the assessment of treatment results in retinoblastoma tumour, especially in macular tumours unresponsive to chemotherapy.

A retrospective study reviewing medical records of 557 retinoblastoma patients for evaluation of the change in regression patterns following chemoreduction (Palamar et al. 2011) showed that most of the changes appeared as non-calcified fish flesh remnant or evolving into a calcified remnant. Most of the changes occurs in the first 6 months after the last cycle of chemoreduction. It is therefore important to frequently follow the tumour
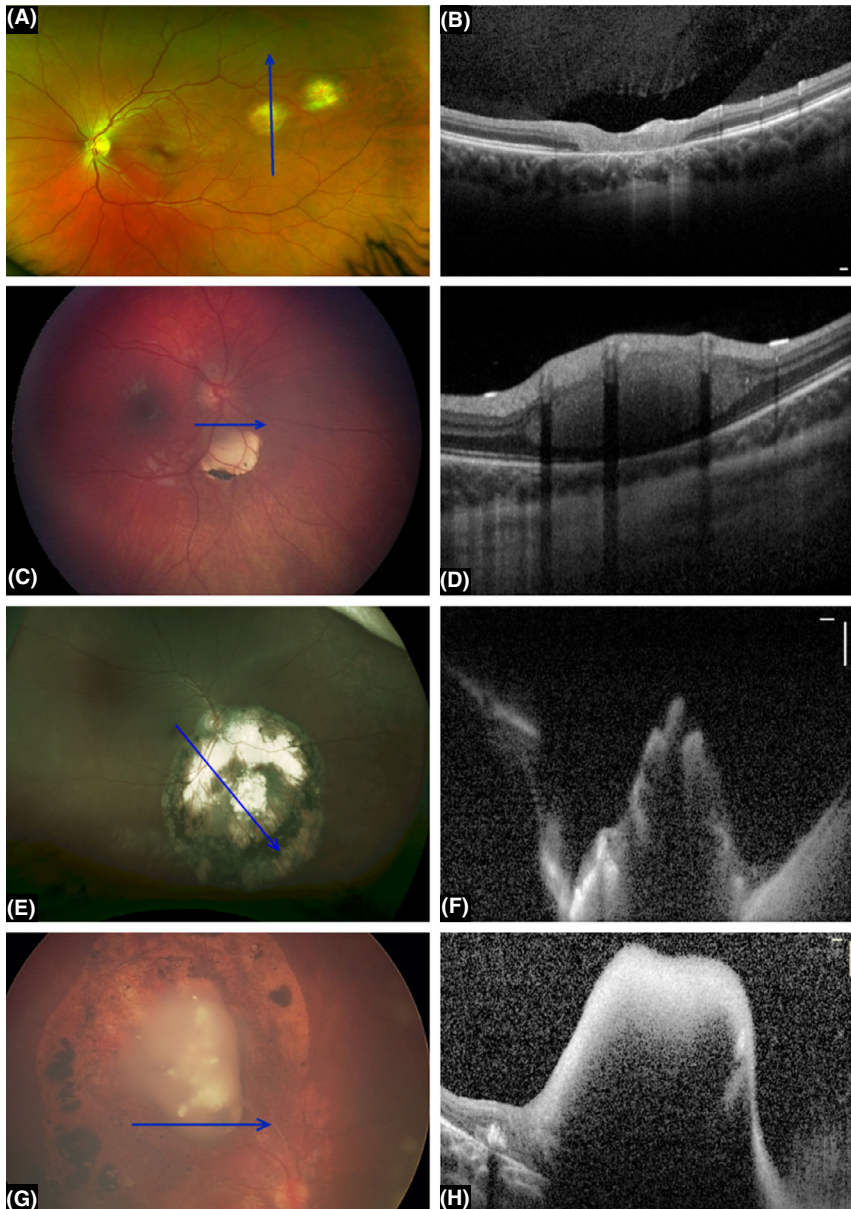
Fig. 4. Fundus picture and OCT scan of patients with inactive tumours (retinomas). *Flat retinoma – Patient SH2:* (A,B) Tumour of the left eye; Irregular surface with flat central remnant is seen in OCT (Heidelberg). *Fish flesh retinoma* – Fundus picture and Heidelberg OCT of *Patient SH1:* (C, D) At diagnosis and after chemotherapy and partial laser treatment, the tumour did not change; a retinoma like mass was still observed in the right eye. After a longer follow-up over time, it got smaller in size similar to observations as in regression type 2. *Calcified retinoma* – (E,F) Fundus picture and Heidelberg OCT of *Patient SH7*. Endophytic tumour of the right eye, located inferiorly to the optic nerve. The lesion was discovered during a routine examination for eye glasses prescription in a 61-year-old woman, without any treatment and appeared stable during follow up. *Mixed retinoma* – Fundus picture and Heidelberg OCT of *Patient SH9:* (G,H) Endophytic tumour with fish flesh tissue and calcification detected in the right eye of a 2-year-old girl whose left eye presented a retinoblastoma group D. No change was noticed during the follow-up. This eye received no treatment. The (Heidelberg) OCT shows a homogenous mass with smooth surface and rare calcifications.

regression patterns after chemotherapy, especially regression types 2 and 3, because of their relapsing potential over time (Palamar et al. 2011). These changes can also be seen in tumours without any additional treatments after

chemoreduction. Others have also reported evolution of retinoma over a period of 20 years (Lam et al. 2005).

In 2009, Shields and associates retrospectively evaluated regression patterns following chemoreduction and

adjuvant therapy in medical records of 557 patients (Shields et al. 2009). In that study they reported a correlation between regression types and tumour thickness. Tumours with a thickness of less than 3 mm evolved more often in a regression pattern type 4; whereas those with 3–8 mm regressed to type 3 or 4 and those with a thickness of more than 8 mm developed into a regression pattern type 1 or 3. Results also showed that macular location, older age, foveolar proximity, lack of consolidation and larger tumour base were the factors predictive of regression pattern type 3. For regression pattern type 4, those factors were familial hereditary pattern, greater foveolar distance, tumour consolidation and smaller tumour base. Most recently, Chawla and colleagues reported similar results (Chawla et al. 2016).

The real benefits of OCT imaging are most useful during follow-up sessions where treatment effects, regression patterns and possible tumour recurrences have to be visualized and diagnosed. However, we were able to identify a number of important limitations for the OCT imaging of Rb. The far peripheral lesions are not accessible due to an unsatisfactory image quality. Furthermore, only the top part of the volume is accessible in large masses and no details can be obtained from regions beneath calcification due to a rapid attenuation of signal. MRI and ultrasonography are used for the management of bigger tumours as a part of standard of care (Dimaras et al. 2015). Another limitation to this optical technique is that it depends on the transparency of the media (Dimaras & Corson 2019).

Shields and associates (Shields et al. 2005) described in a previous study that internal reflectivity of calcified tumours may be higher showing a back scattering response and a much denser shadow behind the layers of the tumour. We observed these features in most of the tumours containing calcifications.

Although, the primary aim of the current study was to demonstrate OCT images of active and inactive Rb tumours, we additionally tried to distinguish between them solely with OCT imaging. We hypothesized that the active Rb tumours will be characterized with typical OCT imaging-specific features (such as vascularization and internal reflectivity) that will help distinguish them from inactive Rb

tumours. Unfortunately, we were not able to identify these features with the OCT systems used for this study. Thus, based on the images obtained in the present study, OCT alone is not able to objectively differentiate between active and inactive retinoblastoma tumours. Hence, a clinician's judgement and follow-up over time are still required.

In our case series with calcified regression pattern types (types I and III, Fig. 3B and F), OCT demonstrated black lesions with strong light scattering. Although this visual feature is typical for calcification, it is not unique or exclusive to calcification. Similar black lesions (opaque regions with shadow effect) are also observed in blood vessels. We distinguished calcification from blood vessels using en-face OCT projections and fundus images, where we almost certainly excluded the possibility of blood vessels in specific areas. To visualize blood vessels with a better sensitivity, in our concurrent work we implemented an angiographic capability in our handheld OCT for mapping of blood vasculature in the vicinity of Rb tumours and retinomas (Nadiarnykh et al. 2019).

The results of current literature are promising. However, the number of cases studied remains modest in combination with a high heterogeneity in patients. Moreover, there is a high variability in morphology of affected retinal layers with variable features between different patients. Similar to the findings of Soliman et al. (2017) we observed the value of OCT imaging in precise localization of tumour masses and regression patterns in the fovea region. In some cases, this information might be useful for the treatment and follow-up decisions with respect to the potential for visual functionality.

Conclusion

Handheld swept-source optical coherence tomography is a relatively new technique to obtain images of the retina in retinoblastoma patients, especially in paediatric patients (aged 0–4) examined under general anaesthesia. Based on our results we suggest that OCT alone cannot make a reliable distinction between active and inactive retinoblastoma tumours. However, handheld OCT adds useful information to the established imaging techniques in the monitoring and follow-up of

retinoblastoma patients, especially in the visualizing and the evaluation of different regression patterns.

Ethical considerations

All the patients included in the current study gave an informed consent. The study protocol was approved by the Medical Ethics Committee (METC) of Amsterdam UMC, location VUMC (METC-nr: 2014.405) in the Netherlands and by the Swiss Federal Department of Health (authorization #2016-00149). All procedures performed involving human participants were in accordance with the ethical standards of the institutional and/or national research committee and with the 1964 Helsinki declaration and its later amendments or comparable ethical standards.

References

Abouzeid H, Balmer A, Moulin AP et al. (2012): Phenotypic variability of retinocytomas: preregression and postregression growth patterns. Br J Ophthalmol 96: 884–889.

Abramson DH, Gerardi CM, Ellsworth RM, McCormick B, Sussman D & Turner L (1991): Radiation regression patterns in treated retinoblastoma: 7 to 21 years later. J Pediatr Ophthalmol Strabismus 28: 108–112.

Abstracts of the Netherlands Ophthalmological Society (NOG) Annual Congress, 27–28 March 2019, Maastricht, The Netherlands. Acta Ophthalmologica 97 (S262): 1–44.

Berry JL, Cobrinik D & Kim JW (2016): Detection and intraretinal localization of an 'Invisible' retinoblastoma using optical coherence tomography. Ocul Oncol Pathol 2: 148–152.

Cao C, Markovitz M, Ferenczy S & Shields CL (2014): Hand-held spectral-domain optical coherence tomography of small macular retinoblastoma in infants before and after chemotherapy. J Pediatr Ophthalmol Strabismus 51: 230–234.

Chawla B, Jain A, Seth R, Azad R, Mohan VK, Pushker N & Ghose S (2016): Clinical outcome and regression patterns of retinoblastoma treated with systemic chemoreduction and focal therapy: a prospective study. Indian J Ophthalmol 64: 524–529.

Dimaras H & Corson TW (2019): Retinoblastoma, the visible CNS tumor: a review. J Neurosci Res 97: 29–44.

Dimaras H, Khetan V, Halliday W et al. (2008): Loss of RB1 induces non-proliferative retinoma: increasing genomic instability correlates with progression to retinoblastoma. Hum Mol Genet 17: 1363–1372.

Dimaras H, Corson TW, Cobrinik D et al. (2015): Retinoblastoma. Nat Rev Dis Primers 1: 15021.

Dunphy EB (1964): The story of retinoblastoma. Am J Ophthalmol 58: 539–552.

Fabian ID, Puccinelli F, Gaillard MC, Beck-Popovic M & Munier FL (2017): Diagnosis and management of secondary epipapillary retinoblastoma. Br J Ophthalmol 101: 1412–1418.

Gaillard MC, Houghton S, Stathopoulos C & Munier FL (2018): OCT-guided management of subclinical recurrent retinoblastoma. Opthal Genet 39: 338–343.

Gallie BL, Ellsworth RM, Abramson DH & Phillips RA (1982): Retinoma: spontaneous regression of retinoblastoma or benign manifestation of the mutation? Br J Cancer 45: 513–521.

Haye C, Desjardins L, Elmaleh C, Schlienger P, Zucker JM & Laurent M (1989): Prognosis and treatment of retinoblastoma, 105 cases treated at Institut Curie. Ophthal Ped Genet 10: 151–155.

Jenkinson H (2015): Retinoblastoma: diagnosis and management—the UK perspective. Arch Dis Child 100: 1070–1075.

Lam A, Shields CL, Manquez ME & Shields JA (2005): Progressive resorption of a presumed spontaneously regressed retinoblastoma over 20 years. Retina 25: 23: 0–231.

Lee H, Proudlock FA & Gottlob I (2016): Pediatric optical coherence tomography in clinical practice-recent progress. Invest Ophthalmol Vis Sci 57: 69–79.

Linn Murphree A (2005): Intraocular retinoblastoma: the case for a new group classification. Ophthalmol Clin North Am 18: 41–53.

Malik K, Welch RJ & Shields CL (2018): Hand-held optical coherence tomography monitoring of chemoresistant retinoblastoma. Retin Cases Brief Rep. https://www.doi.org/10.1097/ICB.0000000000000714 [Epub ahead of print].

Mallipatna A, Vinekar A, Jayadev C et al. (2015): The use of handheld spectral domain optical coherence tomography in pediatric ophthalmology practice: Our experience of 975 infants and children. Indian J Ophthalmol 63: 586–593.

Moll AC (1996): Thesis: Epidemiological Aspects of Retinoblastoma in the Netherlands. ISBN: 978909009773: 2.

Moll AC, Kuik DJ, Bouter LM, Bezemer P, Koten JW, Imhof S, Kuyt B & Tan K (1997): Incidence and survival of retinoblastoma in the Netherlands: a register based study 1862 – 1995. Br J Ophthalmol 81: 559–562.

Nadiarnykh O, Davidoiu V, Gräfe MGO, Bosscha M, Moll AC & de Boer JF (2019): Phase-based OCT angiography in diagnostic imaging of pediatric retinoblastoma patients: abnormal blood vessels in post-treatment regression patterns. Biomed Opt Exp 10: 2213–2226.

Palamar M, Thangappan A & Shields CL (2011): Evolution in Regression Patterns

Following Chemoreduction for Retinoblastoma. Arch Ophthalmol **129**: 727–730.

Park K, Soufi K & Shields CL (2017): Clinically invisible retinoblastoma recurrence in an infant. Retina Cases Brief Rep **13**: 108–110.

Rootman DB, Gonzalez E, Mallipatna A et al. (2013): Hand-held high-resolution spectral domain optical coherence tomography in retinoblastoma: clinical and morphologic considerations. Br J Ophthalmol **97**: 59–65.

Saktanasate J, Vongkulsiri S & Khoo CT (2015): Invisible retinoblastoma. JAMA Ophthalmol **133**: e151123.

Scott AW, Farsiu S, Eynedi LB, Wallace DK & Toth CA (2009): Imaging the infant retina with a hand-held spectral-domain optical coherence tomography device. Am J Ophthalmol **147**: 364–373.

Shah PK, Narendran V, Manayath GJ & Chowdhary S (2011): Atypical retinocytoma with diffuse vitreous seeds: An insight. Oman Journal of Ophthalmology **4**: 81–83.

Shields CL & Shields JA (2017): The American society of retina specialists 2016 founders award lecture—retinal tumors: understanding clinical features, OCT morphology, and therapy. J Vitreoretin Dis **1**: 10–23.

Shields CL, Mashayekhi A, Luo CK, Materin MA & Shields JA (2004): Optical coherence tomography in children: analysis of 44 eyes with intraocular tumors and simulating conditions. J Pediatr Ophthalmol Strabismus **41**: 338–344.

Shields CL, Materin MM & Shields JA (2005): Review of optical coherence tomography for intraocular tumors. Current Opinion in Ophthalmology 16: 141 **15**: 4.

Shields CL, Palamar M, Sharma P, Ramasubramanian A, Leahey A, Meadows AT & Shields JA (2009): Retinoblastoma regression patterns following chemoreduction and adjuvant therapy in 557 tumors. Arch Ophthalmol **127**: 282–290.

Shields CL, Manalac J, Das C, Saktanasate J & Shields JA (2015): Review of spectral domain-enhanced depth imaging optical coherence tomography of tumors of the retina and retinal pigment epithelium in children and adults. Indian J Ophthalmol **63**: 128–132.

Singh AD, Garway-Heath D, Love S, Plowman PN, Kingston JE & Hungerford JL (1993): Relationship of regression pattern to recurrence in retinoblastoma. Br J Ophthalmol **77**: 12–16.

Sobin LH, Gospodarowicz MK & Wittekind CH (2010): TNM classification of malignant tumours — 7th ed. Blackwell Publishing Ltd, ISBN 978-1 **444**: 3–3241.

Soliman SE, VandenHoven C, MacKeen LD, Héon E & Gallie BL (2017): Optical coherence tomography-guided decisions in retinoblastoma management. Ophthalmology **124**: 859–872.

Stathopoulos C, Gaillard MC, Puccinelli F, Maeder P, Hadjistilianou D, Beck-Popovi M & Munier FL (2018): Successful conservative treatment of massive choroidal relapse in 2 retinoblastoma patients monitored by ultrasound biomicroscopy and/or spectral domain optic coherence tomography. Ophthalmic Genet **39**: 242–246.

Yousef YA, Shroff M, Halliday W, Gallie BL & Heon E (2012): Detection of optic nerve disease in retinoblastoma by use of spectral domain optical coherence tomography. The American Association for Pediatric Ophthalmology and Strabismus **16**: 481–483.

Yun J, Li Y, Xu CT & Pan BR (2011): Epidemiology and Rb1 gene of retinoblastoma. Int J Ophthalmol **4**: 103–109.

Correspondence:
Nuray A. McNeill-Badalova
Department of Ophthalmology
Amsterdam UMC
location VUMC
De Boelelaan 1117
1007 MB
Amsterdam
The Netherlands
Tel: + 31 20 444 4795
Fax + 31 20 444 4745
Email: n.mcneill@amsterdamumc.nl

Supporting Information

Additional Supporting Information may be found in the online version of this article:

Appendix S1. Table of characteristics for each patient included in the study.
Appendix S2. Figures of fundus and OCT images of patients not presented in the main article.